Stable Potassium Isotopes ($^{41}K/^{39}K$) Track Transcellular and Paracellular Potassium Transport in Biological Systems

John A. Higgins[1*], Danielle Santiago Ramos[2], Stefania Gili[1], Cornelia Spetea[3,4], Scott Kanoski[5], Darren Ha[6], Alicia A. McDonough[6], Jang H. Youn[6]

[1]Department of Geosciences, Princeton University, Princeton, USA
[2]Department of Marine and Coastal Science, Rutgers University, New Brunswick, USA
[3]Department of Biological and Environmental Sciences, University of Gothenburg, Gothenburg, Sweden
[4]Department of Molecular Biology, Princeton University, Princeton, USA
[5]Department of Human and Evolutionary Biology, University of Southern California, Los Angeles, USA
[6]Department of Physiology and Neuroscience, University of Southern California Keck School of Medicine, Los Angeles, USA

Abstract: Here we present measurements of the stable isotope ratios of potassium ($^{41}K/^{39}K$) in three biological systems. We show that the ratio of ^{41}K to ^{39}K varies systematically: between the single-celled green alga *Chlamydomonas reinhardtii* and growth medium; between muscles of both euryhaline and stenohaline marine teleosts and seawater; and between blood plasma and red blood cells, muscles, cerebrospinal fluid, brain tissues, and urine in the terrestrial mammal *Rattus norvegicus*. Considered in the context of our current understanding of K^+ transport in these biological systems, our results provide evidence that the fractionation of K isotopes depends on transport pathway and transmembrane transport machinery: K^+ channels and paracellular transport through tight-junctions favor ^{39}K whereas K^+ pumps and co-transporters exhibit less isotopic fractionation. These results indicate that stable K isotopes can provide unique quantitative insights into the machinery and dynamics of K^+ homeostasis in biological systems.

1. Introduction

As the most abundant cation in archaeal, bacterial, and eukaryotic cells, potassium (K^+) is an essential nutrient in all biological systems. Intracellular K^+, critical for electrical excitability, protein synthesis, energy metabolism, and cell volume regulation, is maintained in eukaryotes at 120-130 mM by the active pumping of K^+ from extracellular fluid (ECF) into the intracellular fluid (ICF) by plasma membrane Na,K-ATP_{ase}. This action maintains ECF K concentration at 3.5-5 mM, establishing a steep transmembrane K^+ gradient that is a key determinant of membrane potential and a source of energy to drive action potentials, control muscle contractility, and power ion transporters (1). The regulation of potassium at both the cellular and organismal level, K^+ homeostasis, is ultimately accomplished at the molecular level by transcellular and paracellular transporters (including ion pumps, channels, co-transporters) moving K across membranes and between cells (2-5). Pumps, channels, and co-transporters are largely conserved across the major domains of life (3, 4, 6). The shared machinery of K^+ transport in biological systems reflects the fundamental role of the electrochemical potential generated by biologically maintained gradients of K^+ across cell membranes. K^+ pumps establish and maintain concentration gradients across cell membranes by moving K^+ (from ECF-ICF) and Na or H (from ICF to ECF) "uphill" against their electrochemical potentials coupled to and driven by the hydrolysis of ATP. K co-transporters couple uphill K transport to "downhill" transport of another ion (e.g., Na or Cl). K^+ channels provide a direct energetically favorable pathway for rapid and yet highly selective transport of K^+ down its electrochemical potential. While much about the machinery of K^+ homeostasis in biological systems is known many quantitative aspects remain enigmatic.(7-9)

In natural systems potassium is made up of two stable (potassium-39 and potassium-41) and one radioactive (potassium-40) isotope. The two stable isotopes of K, ^{39}K and ^{41}K, constitute 93.258% and 6.730% of the total, respectively, resulting in a ratio of $^{41}K/^{39}K$ in nature of ~0.07217. Recent advances in inductively coupled plasma mass spectrometry (ICP-MS) now permit the precise quantification of deviations from the terrestrial ratio resulting from the biogeochemical cycling of potassium in nature with a precision of 1 part in 10,000 (10-12). Here we apply this analytical tool to study K^+ homeostasis in three biological systems – aquatic green alga *Chlamydomonas reinhardtii* (*C. reinhardtii*), a suite of euryhaline and stenohaline marine teleosts, and the terrestrial mammal *Rattus norvegicus* (*R. norvegicus*). The results in each system are interpreted as reflecting K^+ homeostasis under normal (optimal) growth conditions and differences between taking into account that the input ratio (standard medium or diet) is distinct from the terrestrial ratio. The data are presented using standard delta notation in parts per thousand (‰).

$$\delta^{41/39}\mathrm{K} = \left({R_{\mathrm{sample}}^{^{41}\mathrm{K}/^{39}\mathrm{K}}} \Big/ {R_{\mathrm{standard}}^{^{41}\mathrm{K}/^{39}\mathrm{K}}} - 1 \right) \cdot 10^3$$

where $R_{\mathrm{sample}}^{^{41}\mathrm{K}/^{39}\mathrm{K}}$ is the ratio of $^{41}K/^{39}K$ in a sample and $R_{\mathrm{standard}}^{^{41}\mathrm{K}/^{39}\mathrm{K}}$ is the $^{41}K/^{39}K$ of the standard). For plants the standard is the $^{41}K/^{39}K$ of the growth medium, whereas for marine teleosts it is the $^{41}K/^{39}K$ of seawater. For *R. norvegicus*, we report the data in one of two ways. To explore total body K^+ homeostasis we report the $^{41}K/^{39}K$ of K excretory losses normalized to the $^{41}K/^{39}K$ of the diet whereas to examine the partitioning of K isotopes between extracellular and intracellular compartments we report the $^{41}K/^{39}K$ of tissues relative to the $^{41}K/^{39}K$ of blood plasma or cerebrospinal fluid (CSF). K isotope fractionation factors are calculated as ratios of isotope ratios (e.g. $\alpha_{\mathrm{medium/cell}} = [^{41}K/^{39}K_{\mathrm{medium}}] / [^{41}K/^{39}K_{\mathrm{cell}}]$) and reported as ε values (in ‰) where $\varepsilon_{\mathrm{medium/cell}} = \alpha_{\mathrm{medium/cell}} - 1$.

2. Results

Results for the freshwater algae *C. reinhardtii,* (Figure 1) show that the $\delta^{41}K$ value of the whole cell is 1.2±0.07‰ lower than the $\delta^{41}K$ value of the growth medium (0‰ by definition) (95% confidence; $P = 4.5\times10^{-5}$).

Results for white muscle tissue from a suite of stenohaline and euryhaline marine teleosts, reported relative to the $^{41}K/^{39}K$ of seawater ($\delta^{41}K_{\mathrm{seawater}}$ = 0‰) are shown in Figure 2a. The total range in muscle $\delta^{41}K$ values is ~2‰ (+1‰ to -1‰). Stenohaline species including *Gadus morhua* (Atlantic Cod), *Peprilus striacanthus* (Butterfish), Xiphias gladius (Swordfish), *Pseudopleuronectes americanus* (Winter Flounder), and *Hippoglossus stenolepis* (Pacific Halibut) are characterized by $\delta^{41}K_{\mathrm{seawater}}$ values that are uniformly negative whereas the euryhaline species *Oncorhynchus kisutch* (Coho Salmon), *Oncorhynchus tshawytscha* (King Salmon), and *Oncorhynchus nerka* (Sockeye Salmon) are characterized by $\delta^{41}K_{\mathrm{seawater}}$ values that are close to zero or positive. When species are grouped by salinity tolerance, average measured $\delta^{41}K_{\mathrm{seawater}}$ values of the two groups are -0.58±0.09‰, and 0.29±0.18‰ for stenohaline and euryhaline species, respectively (95% confidence; $P = 1.4\times10^{-10}$).

Results for *R. norvegicus* are shown in Figures 3-5. Measured $\delta^{41}K$ values of both urine and feces, normalized to the $\delta^{41}K$ value of the rat diet ($\delta^{41}K_{\mathrm{diet}}$), indicate preferential net uptake of ^{39}K relative to ^{41}K across the gut epithelium leading to a positive $\delta^{41}K_{\mathrm{diet}}$ value in feces (+0.19±0.09‰, 95% confidence; $P = 0.037$; Fig. 3) and

slightly negative $\delta^{41}K_{diet}$ value in urine (-0.09±0.10‰, 95% confidence; P = 0.1895). Measurements of K isotopes of various tissues in *R. norvegicus* (except brain tissues) are normalized to the $\delta^{41}K$ value of the blood plasma ($\delta^{41}K_{plasma}$), as this represents the extracellular K concentration bathing the tissues. For brain tissues, measured $\delta^{41}K$ values are normalized to CSF ($\delta^{41}K_{CSF}$) for the same reason.

The overall range in $\delta^{41}K_{plasma}$ values between different tissues and fluids is ~1‰ (Fig 4,5); $\delta^{41}K$ values of the following tissues are elevated in ^{41}K relative to blood plasma (positive $\delta^{41}K_{plasma}$ values): red blood cells (+0.40±0.08‰, P = 0.005), heart (+0.55±0.15‰, P = 0.0047), liver (+0.30±0.05‰, P = 0.01), and soleus muscle (+0.17±0.03‰, P = 0.05). Similarly, brain tissues are elevated in ^{41}K relative to CSF (positive $\delta^{41}K_{CSF}$ values): cerebrum (+0.34±0.15‰, P = 0.012), spinal cord (+0.30±0.17‰, P = 0.026), and cerebellum (+0.21±0.11‰, P = 0.037). In contrast, urine (-0.50±0.10‰, P = 0.0019) and CSF (-0.59±0.12‰, $P = 6.2 \times 10^{-5}$) are characterized by negative $\delta^{41}K_{plasma}$ values. In another category are tissues with $\delta^{41}K_{plasma}$ values that are statistically indistinguishable from zero including: kidneys (+0.07±0.07‰, P = 0.31), adipose tissue (+0.01±0.08‰, P = 0.92), extensor digitorum longus (EDL, +0.17±0.11‰, P= 0.099) gastrocnemius (+0.01±0.15‰, P = 0.92), and tibialis anterior (TA, +0.09±0.1‰, P = 0.30).

3. Discussion

The shared machinery of K^+ transport in biological systems suggests that the variability in stable K isotopes observed in algae, marine teleosts, and terrestrial mammals reflects the extent to which this machinery (tight junctions, channels, pumps, and co-transporters) discriminates between ^{39}K and ^{41}K and how that machinery is assembled into a homeostatic system. The extent to which different K^+ transporters discriminate between ^{39}K and ^{41}K will, in turn, depend on the mechanics and selectivity of the transporter. For example, the ~25% difference in ionic radius between Na^+ and K^+ is believed to play a role in the strong selectivity of K^+ channels for K^+ over Na^+ and Christiansen et al. (13) proposed that a size difference of 0.0035% between ^{41}K and ^{39}K could result in a ~1‰ K isotope effect ($\varepsilon_{channel}$) due to size selectivity. However, K^+ channels are not rigid structures and have been shown to exhibit considerable flexibility (13), suggesting that K isotopic fractionation by size selection may not be straightforward.

Desolvation of K^+ during the binding to an active site in K^+ pumps/cotransporters or through interaction with functional groups (e.g. carbonyl) in K^+ channels and pores in tight-junctions represents another potential source of K isotope fractionation that favors ^{39}K due to the lower energetic costs associated with the removal of the hydration shell from ^{39}K. Molecular dynamic simulations indicate that kinetic isotope effects associated with desolvation ($\varepsilon_{desolvation}$) may be as large as ~2.5‰ (14). However, the magnitude of this isotope effect will depend on extent to which desolvation is complete, the bonding

environment of the K^+-coordinating ligands on the transporter (15), as well as whether the K^+ bound to the transporter subsequently isotopically equilibrates with the fluid through solvation-desolvation isotope exchange reactions. Although isotopic equilibration between bound and free K^+ may still be associated with isotopic fractionation, the magnitudes of these effects tend to be significantly smaller (e.g. <1‰) and controlled by bonding environment (e.g. anion charge and bond length; (10, 16, 17)).

Given the potential for K isotope fractionation associated with desolvation and/or size selectivity and the mechanics of K^+-transport by pumps, co-transporters, tight-junctions, and channels, we hypothesize that different classes of K^+ transporters will be associated with different K isotope effects. We propose that K^+ transport by channels and tight junctions will be associated with large K isotope effects favoring ^{39}K ($\varepsilon_{channel\ or\ TJ}$ > 1‰) compared to K^+ transport by pumps and co-transporters ($\varepsilon_{pump\ or\ co\text{-}transport}$ ~ 0‰). K^+ transport through channels and tight junctions is rapid (near the limit of diffusion; (18)) and appears to involve either partial or full desolvation (19-21). In contrast, K^+ transport through pumps and co-transporters is relatively slow (per unit transporter, (13)), requires the simultaneous binding of multiple ions (e.g. 2 K^+ ions in the case of Na,K-ATPase), and is associated with mechanisms of self-correction that prevent the pump cycle from proceeding if incorrect ions bind to the ion pocket (22). These effects will tend to increase the amount of time K^+ is bound to the ion pocket before occlusion and may lead to partial or full equilibration of K isotopes between the ion pocket and the fluid. As equilibrium K isotope effects tend to be small (10, 16, 17), we speculate that K^+ transport by pumps and co-transporters are associated with less fractionation of K isotopes. In the following sections we show how our results for three biological systems are consistent with this hypothesis and speculate on ways in which K isotopes may provide new quantitative insights into K^+ transport and homeostasis in biological systems.

Algae and Higher Plants. As an essential macronutrient in all plants and the most abundant cation in the cytoplasm, K^+ contributes to electrical neutralization of anionic groups, membrane potential and osmoregulation, photosynthesis, and the movements of stomata (3, 23). K^+ transport across plant membranes is mediated by at least six major families of cation transport systems - 3 families of ion channels and 3 families of ion transporters. It is well-established that K^+ channels play prominent roles in K^+ uptake (24). For example, under normal growth conditions ($[K^+]_{ext}$ ~1 mM; (25-27)) K^+ uptake in plants is dominated by transport via inward-rectifying K^+ channels electrically balanced by the ATP-driven efflux of H^+ (28, 29). In higher plants, K^+ channels have also been shown to be involved in translocation (root to stem), and recycling (leaf to root; 25).

Determining the K isotope effect associated with K^+ uptake by K^+-channels in *C. reinhardtii* can be approximated by the difference in $\delta^{41}K$ values between the whole cells and growth medium ($\varepsilon_{in} = \delta^{41}K_{medium} - \delta^{41}K_{cell}$ = ~1.2‰; Figure 1). This result is similar

in sign, though somewhat larger in magnitude, than the K isotope effects estimated by Christensen, Qin, Brown and DePaolo (15) for K^+ transport in higher plants. Those authors analyzed the $\delta^{41}K$ values of the roots, stems, and leaves of *Triticum aestivum* (wheat), *Glycine max* (soy) and *Oryza sativa* (rice) grown under hydroponic conditions and observed systematic differences in the $\delta^{41}K$ value of the different reservoirs. In particular, roots, stems, and leaves exhibited increasingly negative $\delta^{41}K$ values (Figure S1). Compared to the freshwater alga *C. reinhardtii*, quantifying transport-specific K isotope effects in higher plants is more complex as the $\delta^{41}K$ value of each individual compartment (root, stem, leaf) reflects a balance between isotopic sources and sinks (e.g. the $\delta^{41}K$ value of the root will depend on K isotope effects associated with both net K^+ uptake as well as translocation and recycling). Using a model of K isotope mass balance that includes assumptions regarding plant growth and the partitioning of K^+ fluxes between translocation and recycling, Christensen, Qin, Brown and DePaolo (15) estimated large K isotope effects for uptake (ε_{in} ~0.7 to 1.0‰) and translocation from root to stem (~0.6‰), but smaller isotopic effects (0 to 0.2‰) for translocation of K^+ from stem to leaf and recycling of K^+ from leaf to root.

Taken together, the results from algae and higher plants indicate that K^+ uptake in these systems – a process dominated K^+ channels – is associated with a large K isotope effect (ε_{in} ~0.7 to 1.2‰). The ~0.6‰ K isotope effect associated with translocation from root to stem is also consistent with transport by K^+ channels (30). In contrast, translocation and recycling of K^+ from leaf to root, a process that also involves K^+ channels (31, 32), does not appear to fractionate K isotopes. This could be due to the increased importance of other types of K^+ transporters in this process, a reduction in the expression of K isotope fractionation by channels associated with translocation due to rapid internal recycling of K^+ between stem and leaf (compared to K^+ transport from root to stem), or some combination of the two.

Stenohaline and Euryhaline Marine Teleosts. K^+ homeostasis in both euryhaline and stenohaline marine teleosts is linked to ionic and osmotic regulation. While K^+ sources include ingestion of seawater and diet (33), by far the largest K^+ source is transport across the gills (34), which are permeable to monovalent cations (Na^+, K^+) and anions (Cl^-). Teleosts balance this salt intake by actively secreting Na^+, K^+ and Cl^- through mitochondria-rich cells (MRCs) of the gills and paracellularly through tight-junction proteins (occludins, claudins) in the gill epithelium (35). Specifically, Na^+, K^+ and Cl^- enter the MRC from the blood side via a basolateral Na^+, K^+, $2Cl^-$ transporter (NKCC) driven by the inward directed Na^+ gradient created by basolateral Na,K-ATPase; Na^+ is recycled back to the blood via the Na,K-ATPase and secreted into seawater via “leaky” tight junction proteins (claudin 10; (36)); K^+ is either 1) secreted across the apical membrane into the seawater through ROMK channels or 2) recycled back to the blood via Kir channels while Cl^- is secreted across the apical membrane via CFTR channels (5,

35). Both stenohaline and euryhaline marine teleosts possess this capability but euryhaline marine teleosts have evolved the ability to adapt this machinery to a wide range of water salinities by adjusting expression of NKCC, ROMK and tight junction claudins (5, 36-38).

In seawater adapted stenohaline and euryhaline marine teleosts, K^+ homeostasis can be approximated as a balance between gain of K^+ across tight-junctions in the gill epithelium and loss of K^+ through apical ROMK channels in MRCs ((5); Fig. 2b). Other potential sources and sinks of K^+ including the ingestion of seawater, diet, and excretion are either small compared to the fluxes of K^+ across the gills (34) or transient in nature and unlikely to explain the systematic difference we observe between the $\delta^{41}K_{seawater}$ values of stenohaline and euryhaline teleosts. Furthermore, as most of the total K^+ content of teleosts resides in muscle tissue, the $\delta^{41}K_{seawater}$ value of the muscle can be used as a reasonable approximation of the $\delta^{41}K_{seawater}$ value of the whole organism (Fig. 2b). At steady state, the $\delta^{41}K_{seawater}$ value of the whole organism (equation 1 in Figure 2b) will reflect the balance between K isotope effects (if any) associated with K^+ sources (paracellular transport across the gills) and K^+ sinks (transcellular transport through ROMK channels in MRCs). Critically, the fractionation of K isotopes associated with K^+ sinks (transcellular K^+ transport across MRCs) depends on the cycling of K^+ within MRCs described above, in particular, the extent to which K^+ transported into MRCs via the basolateral NKCC transporter and Na,K-ATPase is then secreted to seawater through ROMK channels or recycled back to the blood via Kir channels (f in Fig. 2C; where $f = F_{MRC\text{-}p}/(F_{MRC\text{-}out}+F_{MRC\text{-}p})$). Combining the steady-state equation for whole organism K isotope mass-balance with a similar equation for the steady-state cycling of K^+ in MRCs we can derive a simple model for K^+ isotope mass balance for muscle tissue (equation 1 in Figure 2c) that includes intake from seawater into plasma through tight-junction proteins (input), secretion from plasma to seawater across MRCs through Na,K-ATPase/NKCC and ROMK (output), as well as K^+ recycling from MRCs back to plasma and exchange of K^+ between muscle tissue and plasma.

Although the complexity of K^+ homeostasis in marine teleosts does not permit the unique determination of K isotope effects associated with individual transport pathways (e.g. gain through pores in gill tight junctions or loss through apical ROMK channels), the model (equation 1) can be used to define an internally consistent set of K isotope effects that can be compared to the machinery of K^+ homeostasis and the difference in $\delta^{41}K_{seawater}$ values between stenohaline and euryhaline teleosts. First, K appears to be at least partially desolvated during transport through pores in tight-junctions (19) and thus we expect a large K isotope effect associated with the source of K^+ across the gill ($\varepsilon_{gill} > 1$). Second, although we also expect a large K isotope effect associated with K^+ loss through apical ROMK channels ($\varepsilon_{MRC-out} > 1$), the extent to which this isotope effect is expressed will depend on K isotope mass balance within MRC cells: K^+ loss through ROMK channels will be associated with a small K isotope effect (stenohaline marine teleosts) if the recycling efficiency of K^+ within MRCs (f; where $f = F_{MRC\text{-}p}/(F_{MRC\text{-}out}+F_{MRC\text{-}}$

$_p$)) is low and K isotope effects associated with Na,K-ATPase are small ($\varepsilon_{p\text{-}MRC}$ ~ 0‰). Conversely, K^+ loss through ROMK channels will be associated with a large K isotope effect (euryhaline marine teleosts) if either the K isotope effect associated with transport of K^+ into MRCs is larger (e.g. ε_{p-MRC} euryhaline > ε_{p-MRC} stenohaline) or, as shown in Figure 2b, if the recycling efficiency of K^+ within MRCs is higher (i.e. f → 1). In the latter case we can explain the full range of observed $\delta^{41}K$ values in euryhaline and stenohaline marine teleosts using a single set of K isotope effects ($\varepsilon_{channel\ or\ tight\ junction}$ = 0.5 to 2.5‰ and $\varepsilon_{pump\ or\ co\text{-}transporter}$ = ~ 0‰).

Terrestrial Mammals. K^+ homeostasis in terrestrial mammals reflects the balance between K^+ gained from diet and K^+ lost in urine and feces (Figure 3). This balance is largely achieved by the kidneys and colon, which possess a remarkable ability to sense a change in K^+ in the diet and then appropriately adjust K^+ loss in response. ECF (which includes blood plasma), the reservoir through which internal K^+ is exchanged, represents 2% of total body K^+ and is also tightly regulated to maintain membrane potential as indicated by the narrow range of normal ECF [K^+] (~ 3.5 – 5 mEq/L,)(8, 39). Of the remaining 98%, 75% of the K^+ resides in muscle tissues ([K^+] ~ 130 mEq/L) and the remaining 23% in non-muscle tissues. Some tissues, particularly skeletal muscle, are critical to K^+ homeostasis by providing a buffering reservoir of K^+ that can take up K^+ after a meal and altruistically donate K^+ to ECF to maintain blood plasma levels during fasting.

External K isotope mass balance in terrestrial mammals. Assuming that ~80-90% of K in the diet is lost in urine (2) and that the progressive removal of K^+ from the gut of *R. norvegicus* can be described by Rayleigh-type distillation of K isotopes, K^+ uptake in the gut is associated with a K isotope effect (ε_{g-p}; Fig.4) of ~0.3 ± 0.1‰ (40). This K isotope effect leads to feces with a positive $\delta^{41}K_{diet}$ value and urine with a slightly negative $\delta^{41}K_{diet}$ value (Figure 3). K^+ uptake in the gut occurs largely transcellularly through tight-junction proteins in epithelial cells (e.g. claudin-15; (41)) and this transport mechanism likely contributes to the observed K isotope fractionation between diet and ECF (40; Fig. 3). However, while net transport of K^+ in the gut is unidirectional (i.e. gut to plasma), other pathways of K^+ cycling (e.g. paracellular secretion of K^+ from ECF to gut (42)) may also contribute to the observed net K isotope effect (ε_{gut}). Relative to the diet, internal tissues exhibit a 1‰ range from -0.04‰ for the cerebellum to +1.05‰ for the heart (Fig. 3). Assuming an internal K^+ distribution that is 75/15/10 muscle/adipose/other tissues, a reasonable average whole-body $\delta^{41}K_{diet}$ value of *R. norvegicus* is ~+0.5‰. As net uptake of K^+ in the gut prefers ^{39}K, the elevated average whole-body $\delta^{41}K_{diet}$ of *R. norvegicus* requires that there be even greater K isotope fractionation (favoring ^{39}K) associated with K^+ loss in the urine (see below).

*Internal K isotope mass balance in terrestrial mammals***.** As shown in Figures 4 and 5, $\delta^{41}K$ values of the 16 different tissues and fluids analyzed in *R. norvegicus* fall into 3 distinct categories relative to their respective fluid reservoirs ($\delta^{41}K_{plasma}$ or $\delta^{41}K_{CSF}$). Type 1 with positive $\delta^{41}K_{plasma/CSF}$ values: red blood cells, heart, liver, soleus muscle and brain tissues; Type 2 with $\delta^{41}K_{plasma/CSF}$ values that are close to 0: stomach, adipose tissue, kidney, gastrocnemius, EDL and TA muscles and Type 3 with negative $\delta^{41}K_{plasma/CSF}$ values: urine and CSF.

For all cases except urine, the $\delta^{41}K$ values in Figures 4 and 5 can be interpreted as reflecting steady-state K isotope mass balance between the tissue/fluid and the relevant fluid reservoir (blood plasma/ECF or CSF) as the timescale for K^+ turnover in these internal reservoirs is rapid (e.g. 0.9-10%/min; (43, 44)). At isotopic steady state, the $\delta^{41}K$ value of K^+ entering the reservoir will be equal to $\delta^{41}K$ value of K^+ leaving the reservoir. As a result, reservoirs with $\delta^{41}K_{plasma/CSF}$ values that differ from 0‰ require that net K^+ transport in one direction results in greater fractionation of K isotopes than net K^+ transport in the opposite direction. For example, reservoirs with positive $\delta^{41}K_{plasma}$ values (Type 1) including red blood cells, heart, liver, and soleus require that K^+ transport from ICF to plasma or ECF is associated with a larger K isotope effect than K^+ transport from ECF to ICF (e.g. $\varepsilon_{t1-p} \sim \varepsilon_{p-t1} + 0.17 \text{ to } 0.55‰$; Fig. 4). The same relationship (Type 1) is observed between brain tissues and CSF (Fig. 5; $\varepsilon_{t1-CSF} \sim \varepsilon_{CSF-t1} + 0.21 \text{ to } 0.34‰$). Similarly, reservoirs with $\delta^{41}K_{plasma}$ values that are close to 0‰ (Type 2) require that net K^+ transport in both directions does not fractionate K isotopes, i.e., the isotope effects must be of equal magnitude and sign and cancel at steady state (e.g. $\varepsilon_{t2-p} \sim \varepsilon_{p-t2}$; Figure 4). These include kidney, adipose tissue, stomach, and gastrocnemius and TA muscles. Finally, the negative $\delta^{41}K_{plasma}$ values for CSF (Type 3) requires that, at steady-state, net K^+ transport from ECF to CSF through the choroid plexus and blood brain barrier (BBB) is characterized by a K isotope effect that is ~0.6‰ greater than the K isotope effect associated K^+ transport from CSF to ECF (Figure 5).

Linking the observed net K isotope effects associated with different internal reservoirs (e.g. Type 1-3) to the machinery of K^+ homeostasis (channels, pumps, co-transporters, and proteins in tight-junctions) in *R. norvegicus* is complicated by the existence of a host of transporters capable of bidirectional K^+ transport between ECF and ICF. Although much is known about the identity, molecular structure, and mechanisms of various transporters, quantitative information on how each transporter contributes to the gross fluxes of K^+ between internal reservoirs and ECF at steady state is lacking. Of the internal reservoirs studied here, the machinery that regulates K homeostasis in red blood cells (Type 1; + $\delta^{41}K_{plasma}$ values) is perhaps the best understood due to its fundamental role in the regulation of red blood cell volume (45). In red blood cells, elevated intercellular K^+ is maintained by a 'pump-leak' mechanism

where the pump is Na,K-ATP_{ase} (with minor contributions from co-transporters such as NKCC;(46, 47)), and the leak is passive transport through K^+ channels (48). When considered in the context of the measured $\delta^{41}K_{plasma}$ values of RBC this mechanism is consistent with K isotope fractionation associated with K transport in channels that is at least 0.4‰ greater than K isotope fractionation associated with K transport in pumps (Na,K-ATP_{ase}) and co-transporters.

Extrapolating this result to internal reservoirs where the machinery of K^+ homeostasis is more complex and less understood due, in part, to the presence of multiple cell types with distinct functions and internal K^+ cycling, we speculate that all Type 1 reservoirs (red blood cells, heart, liver, and soleus muscle) are broadly characterized by a similar 'pump-leak' mechanism with greater fractionation of K isotopes during K^+ transport from ICF to ECF via channels than K transport from ECF to ICF via pumps and co-transporters. Measured $\delta^{41}K_{plasma}$ values of Type 1 reservoirs are not uniform, however, and the observed variability, from +0.55 ±0.15‰ in heart tissue to +0.17 ±0.03‰ for soleus muscle, likely reflects real differences in 1) K isotope effects associated with transport of K from ICF to ECF (e.g. due to channel-specific K isotope effects or transport of K from ICF to ECF via co-transporters) and/or 2) K isotope effects associated with transport from ECF to ICF (e.g. due to pump/co-transporter-specific K isotope effects or transport of K from ECF to ICF via channels).

Along similar lines we interpret Type 2 reservoirs (EDL, gastrocnemius, and TA muscles, adipose tissue, stomach, and kidney) as cases where any K isotope effects associated with transport from ICF to ECF cancel those associated with transport from ECF to ICF. This could be achieved in a number of different ways; an increased role for pumps/co-transporters for K^+ transport from ICF to ECF or an increased role for channels in K^+ transport from ECF to ICF. For example, there is evidence that the strong inward rectifier K^+ channel (Kir2.1) is involved in K^+ influx in skeletal muscle (49). Isotope effects associated with K^+ influx through these K^+ channels may offset some of the isotope effect of K^+ channels involved in K^+ efflux.

Both Type 3 reservoirs, urine and CSF, are associated with complex pathways of K^+ exchange along the nephron (urine, Fig. 4) and across the blood-brain-barrier and the choroid plexus (CSF, Figure 5) and are considered separately. K^+ in CSF reflects a balance between paracellular and transcellular K^+ transport across endothelial cells at the blood-brain-barrier (BBB) and paracellular K^+ transport of across epithelial cells of the choroid plexus (49). Gross fluxes of K^+ into the brain across the BBB are 4x larger than those associated with the choroid plexus (50), suggesting that the observed net K isotope effects may be largely due to fractionation associated with transport across the BBB. However, K^+ transport from ECF to CSF through the choroid plexus is thought to occur by paracellular routes through pores in tight junctions (Fig. 5), a process that we expect to fractionate K isotopes and thus may contribute to the observed negative $\delta^{41}K_{plasma}$ values for CSF. With regards to K^+ transport across the BBB, both paracellular (through tight-junction pores) and transcellular (through BBB endothelial cells) routes

may be important (49). Again, we expect paracellular K^+ transport through tight junction pores to be associated with a larger K isotope effect whereas any K isotope effects associated with transcellular transport will depend on the internal cycling of K^+ (and associated isotope effects) within endothelial BBB cells (pumps, (51); co-transporters, (52); and channels, (53)). Overall, the observation of large K isotope fractionation associated with the transport of K^+ from plasma to CSF (Fig. 5; $\varepsilon_{p-CSF} = 0.59 \pm 0.12‰$) requires that either 1) there is a large K isotope effect associated with transcellular K^+ transport across endothelial BBB cells or 2) transport of K^+ from plasma to CSF is dominated by paracellular routes in both the choroid plexus and across the BBB.

Unlike the internal K^+ reservoirs discussed above, all of which are interpreted as independent homeostatic systems at steady state with an external fluid (e.g. plasma or CSF), the loss of K^+ through the urine represents the end product of a series of steps each of which can contribute to the net K isotope effect (e.g. Figure 4; $\varepsilon_{p-u} \sim 0.50‰$). These are 1) glomerular filtration, 2) reabsorption along the proximal tubule and the thick ascending limb of the loop of Henle, and 3) secretion and reabsorption by principal and intercalated collecting duct cells. Although a detailed description of the potential K isotope effects associated with each step is beyond the scope of this manuscript, a brief description follows. Glomerular filtration is not expected to fractionate K isotopes as the slit diaphragms freely filter ions and small molecules. A large fraction (~85%) of the filtered K is subsequently reabsorbed in the proximal tubule and thick ascending limb. The residual K^+ is passed along to the collecting ducts where K^+ is added prior to excretion as urine. The addition of K^+ in the collecting ducts occurs transcellularly, via ROMK channels in principal cells and BK channels in intercalated cells (8). However, although we expect K^+ channels to be associated with a large K isotope effect ($\varepsilon_{channel}$ > 1‰), a negative $\delta^{41}K_{plasma}$ value for K^+ secreted from collecting duct cells is not an obvious result; the extent to which any isotopic fractionation associated with these channels is expressed depends on internal K^+ cycling within the principal and intercalated cells in a manner that is analogous to MRCs in marine teleost gills (54).

Ideas and Speculation: The results presented here demonstrate that K^+ homeostasis in biological systems is associated with systematic variability in $^{41}K/^{39}K$ ratios and strongly suggests that K transport through channels and tight-junction proteins is associated with greater fractionation of K isotopes than transport via pumps and co-transporters. However, with the exception of *C. Reinhardtii* where the observed isotopic difference between media and the whole cell can be attributed to a single transport mechanism, our results do not directly constrain the magnitude of the individual K isotope effects associated with the machinery of K transport. Quantifying machinery-specific K isotope effects through a combination of laboratory and numerical approaches (14) is therefore a high-priority for future research. Identification of machinery-specific K isotope effects will lead to improvements in our understanding of the underlying mechanisms of K^+ transport

(and selectively) and may permit the quantification of the K^+ transporters involved in K homeostasis *in situ*.

4. Materials and Methods

C. reinhardtii cultures: The CMJ030 wild type strain was obtained from the Chlamydomonas culture collection www.chlamycollection.org). Tris Phosphate (TP) medium was prepared according to: Gorman, D.S., and R.P. Levine (1965) Proc. Natl. Acad. Sci. USA 54, 1665-1669. The culture at an initial density of 0.5 $x10^5$ cells mL^{-1} was grown in TP under continuous illumination (100 µmol photons m^{-2} s^{-1}) and shaking for four days. Samples (in triplicate) containing 2 $x10^7$ cells (~800 mg) were harvested and washed twice in 5 mM HEPES and 2 mM EDTA before collection and air-drying of the cell pellet. Pelletized cells (~30mg) were digested in screw-capped teflon vials on a hot plate at elevated temperatures (~75 °C) using a 5:2 mixture of HNO_3 (68-70 vol.%) and H_2O_2 (30 vol.%).

Euryhaline and stenohaline marine teleosts: Samples of teleost muscle tissue were sourced from fish markets (Nassau Seafood and Trader Joe's in Princeton, NJ and the Fulton Fish Market in Brooklyn, NY) and research cruises (NOAA NEFSC Bottom Trawl Survey, Fall 2015 and Spring 2015). All teleosts were caught in seawater which has a uniform $\delta^{41}K$ value of +0.12‰ relative to SRM3141a (55). Samples of white dorsal muscle (100 to 3000 mg) were digested on a hot plate at elevated temperatures (~75 °C) or in a high-pressure microwave system (MARS 6) using HNO_3 (68-70 vol.%) H_2O_2 (30 vol.%) in a ratio of 5:2 until complete. Major/minor element analyses for digested samples were carried out at Princeton University using a quadrupole inductively coupled plasma mass spectrometer (Thermo Scientific iCap Q). Concentrations and elemental ratios were determined using externally calibrated standards and average uncertainties (element/element) are ~10%.

R. norvegicus experiments: All rat experiments were approved by the Institutional Animal Care and Use Committees of the University of Southern California. Two series were conducted. Series #1: Male Wistar rats (n=3, 250-275g body weight, Envigo, Indianapolis, IN) were housed in a climate controlled (22-24°C) environment with a 12 hr: 12hr light/dark cycle, and fed casein based normal K^+ diet TD.08267 (Envigo, Indianapolis, IN) and water ad libitum for 11 days. At day 8, rats were placed overnight into metabolic cages (Techniplast, Buguggiate, Italy) with food and water ad libitum for 16-hour collection of urine and feces. On termination day (1:30-3:30PM), rats were anesthetized with an intramuscular (IM) injection of ketamine (80 mg/kg, Phoenix Pharmaceuticals, St. Joseph, MO) and xylazine (8 mg/kg, Lloyd Laboratories, Shenandoah, IA) in a 1:1 ratio. Through a midline incision, the liver, kidneys, heart, fat pads, and stomach (flushed of contents) were removed; blood was collected via cardiac puncture, spun down to separate plasma from RBCs. Then gastrocnemius, soleus, TA, and EDL skeletal muscles were dissected. All tissues were washed in ice-cold TBS to remove excess blood, weighed and snap frozen in liquid nitrogen. Series #2: Male Sprague Dawley rats (n=4, 250-300g, Envigo, Indianapolis, IN) were housed in a climate controlled (22-24°C) environment with a 12 hr: 12hr light/dark cycle and fed grain-based vivarium chow (LabDiet 5001, labdiet.com). CSF extraction procedures are as reported

previously (56). In brief, Rats were deeply anesthetized using a cocktail of ketamine 90mg/kg, xylazine, 2.8 mg/kg, and acepromazine 0.72 mg/kg by intramuscular injection. A needle was lowered to below the caudal end of the occipital skull and the syringe plunger pulled back slowly, allowing the clear CSF to flow into the syringe. After extracting ~100-200 µl of CSF, the needle was raised quickly (to prevent suction of blood while coming out of the cisterna magna) and the CSF dispensed into a microfuge tube and immediately frozen in dry ice and then stored at -80 °C until time of analysis. Following CSF extraction and decapitation, whole brains with 10-15mm spinal cord extension were rapidly removed and immediately flash frozen and stored in -80°C until dissection into spinal cord, cerebrum, and cerebellum for subsequent digestion and K isotopic analysis.

Ion chromatography and isotope ratio mass-spectrometry: K was purified for isotopic analyses using an automated high-pressure ion chromatography (IC) system. The IC methods utilized here followed those previously described in (10, 11). The accuracy of our chromatographic methods was verified by purifying and analyzing external standards (SRM3141a and SRM70b) alongside unknown samples. Purified aliquots of K were analyzed in 2% HNO_3 for their isotopic compositions on a Thermo Scientific Neptune Plus multi-collector inductively coupled plasma mass spectrometer (MC-ICP-MS) at Princeton University, using previously published methods (11, 55). The external reproducibility of our protocols (chromatography and mass spectrometry) was determined through replicate measurements of international standards. Measured values of SRM70b, reported relative to SRM3141 ($\delta^{41}K_{SRM3141}$) are -0.57 ± 0.17‰ (2σ; N = 59), indistinguishable from published values (10, 12, 55). For samples analyzed once (chromatography and mass spectrometry), reported errors are the 2σ uncertainties of the external standard. In cases where samples were analyzed multiple times, reported errors in are twice the standard error of the mean (2 S.E. or 95% confidence).

Acknowledgments

Cornelia Spetea acknowledges the sabbatical program at the Faculty of Science, University of Gothenburg, and thanks Martin C. Jonikas for the *Chlamydomonas* experiments performed in his laboratory at Princeton University. John Higgins, Alicia McDonough, and Jang Youn thank the University Kidney Research Organization (UKRO) for financial support.

References

1. A. A. McDonough, J. H. Youn, Potassium Homeostasis: The Knowns, the Unknowns, and the Health Benefits. *Physiology* **32**, 100-111 (2017).
2. R. Agarwal, R. Afzalpurkar, J. S. Fordtran, Pathophysiology of potassium absorption and secretion by the human intestine. *Gastroenterology* **107**, 548-571 (1994).
3. M. Gierth, P. Mäser, Potassium transporters in plants–involvement in K+ acquisition, redistribution and homeostasis. *FEBS letters* **581**, 2348-2356 (2007).

4. J. H. Youn, A. A. McDonough, Recent advances in understanding integrative control of potassium homeostasis. *Annual review of physiology* **71**, 381-401 (2009).
5. F. Furukawa, S. Watanabe, S. Kimura, T. Kaneko, Potassium excretion through ROMK potassium channel expressed in gill mitochondrion-rich cells of Mozambique tilapia. *American Journal of Physiology-Regulatory, Integrative and Comparative Physiology* **302**, R568-R576 (2012).
6. J. Stautz *et al.*, Molecular Mechanisms for Bacterial Potassium Homeostasis. *Journal of Molecular Biology* **433** (2021).
7. M. L. Gumz, L. Rabinowitz, C. S. Wingo, An Integrated View of Potassium Homeostasis. *N Engl J Med* **373**, 60-72 (2015).
8. A. A. McDonough, J. H. Youn, Potassium Homeostasis: The Knowns, the Unknowns, and the Health Benefits. *Physiology (Bethesda)* **32**, 100-111 (2017).
9. M. Greenlee, C. S. Wingo, A. A. McDonough, J. H. Youn, B. C. Kone, Narrative review: evolving concepts in potassium homeostasis and hypokalemia. *Annals of internal medicine* **150**, 619-625 (2009).
10. D. P. S. Ramos, L. E. Morgan, N. S. Lloyd, J. A. Higgins, Reverse weathering in marine sediments and the geochemical cycle of potassium in seawater: Insights from the K isotopic composition (K-41/K-39) of deep-sea pore-fluids. *Geochimica Et Cosmochimica Acta* **236**, 99-120 (2018).
11. L. E. Morgan *et al.*, High-precision K-41/K-39 measurements by MC-ICP-MS indicate terrestrial variability of delta K-41. *Journal of Analytical Atomic Spectrometry* **33**, 175-186 (2018).
12. K. Wang, S. B. Jacobsen, An estimate of the Bulk Silicate Earth potassium isotopic composition based on MC-ICPMS measurements of basalts. *Geochimica Et Cosmochimica Acta* **178**, 223-232 (2016).
13. B. Roux, Ion channels and ion selectivity. *Essays in biochemistry* **61**, 201-209 (2017).
14. A. E. Hofmann, I. C. Bourg, D. J. DePaolo, Ion desolvation as a mechanism for kinetic isotope fractionation in aqueous systems. *Proceedings of the National Academy of Sciences* **109**, 18689-18694 (2012).
15. J. N. Christensen, L. Qin, S. T. Brown, D. J. DePaolo, Potassium and calcium isotopic fractionation by plants (soybean [Glycine max], rice [Oryza sativa], and wheat [Triticum aestivum]). *ACS Earth and Space Chemistry* **2**, 745-752 (2018).
16. W. Li, K. D. Kwon, S. Li, B. L. Beard, Potassium isotope fractionation between K-salts and saturated aqueous solutions at room temperature: Laboratory experiments and theoretical calculations. *Geochimica et Cosmochimica Acta* **214**, 1-13 (2017).
17. H. Zeng *et al.*, Ab Initio Calculation of Equilibrium Isotopic Fractionations of Potassium and Rubidium in Minerals and Water. *Acs Earth and Space Chemistry* **3**, 2601-2612 (2019).
18. B. Hille, *Ion channels of excitable membranes* (Sinauer, Sunderland, Mass., 2001).
19. H. Yu, S. Y. Noskov, B. Roux, Two mechanisms of ion selectivity in protein binding sites. *Proceedings of the National Academy of Sciences* **107**, 20329-20334 (2010).
20. W. Kopec *et al.*, Direct knock-on of desolvated ions governs strict ion selectivity in K^+ channels. *Nature chemistry* **10**, 813-820 (2018).

21. S. Berneche, B. Roux, A microscopic view of ion conduction through the K+ channel. *Proceedings of the National Academy of Sciences of the United States of America* **100**, 8644-8648 (2003).
22. H. Rui, P. Artigas, B. Roux, The selectivity of the Na^+/K^+-pump is controlled by binding site protonation and self-correcting occlusion. *Elife* **5**, e16616 (2016).
23. J. Marchand, P. Heydarizadeh, B. Schoefs, C. Spetea, "Chloroplast Ion and Metabolite Transport in Algae" in Photosynthesis in Algae: Biochemical and Physiological Mechanisms, A. W. D. Larkum, A. R. Grossman, J. A. Raven, Eds. (Springer International Publishing, Cham, 2020), 10.1007/978-3-030-33397-3_6, pp. 107-139.
24. A. Lebaudy, A.-A. Véry, H. Sentenac, K^+ channel activity in plants: genes, regulations and functions. *FEBS letters* **581**, 2357-2366 (2007).
25. B. Malhotra, A. D. Glass, Potassium fluxes in Chlamydomonas reinhardtii (I. Kinetics and electrical potentials). *Plant physiology* **108**, 1527-1536 (1995).
26. E. Epstein, D. Rains, O. Elzam, Resolution of dual mechanisms of potassium absorption by barley roots. *Proceedings of the National Academy of Sciences of the United States of America* **49**, 684 (1963).
27. L. V. Kochian, W. J. Lucas, Potassium transport in corn roots: I. Resolution of kinetics into a saturable and linear component. *Plant Physiology* **70**, 1723-1731 (1982).
28. R. E. Hirsch, B. D. Lewis, E. P. Spalding, M. R. Sussman, A role for the AKT1 potassium channel in plant nutrition. *Science* **280**, 918-921 (1998).
29. D. T. Britto, H. J. Kronzucker, Cellular mechanisms of potassium transport in plants. *Physiologia Plantarum* **133**, 637-650 (2008).
30. F. Gaymard *et al.*, Identification and disruption of a plant shaker-like outward channel involved in K^+ release into the xylem sap. *Cell* **94**, 647-655 (1998).
31. B. Lacombe *et al.*, A shaker-like K^+ channel with weak rectification is expressed in both source and sink phloem tissues of Arabidopsis. *The Plant Cell* **12**, 837-851 (2000).
32. G. Pilot *et al.*, Guard cell inward K^+ channel activity inarabidopsis involves expression of the twin channel subunits KAT1 and KAT2. *Journal of Biological Chemistry* **276**, 3215-3221 (2001).
33. C. P. Hickman Jr, Ingestion, intestinal absorption, and elimination of seawater and salts in the southern flounder, Paralichthys lethostigma. *Canadian journal of zoology* **46**, 457-466 (1968).
34. J. Maetz, Seawater teleosts - evidence for a sodium-potassium exchange in branchial sodium-excreting pump. *Science* **166**, 613-& (1969).
35. D. H. Evans, P. M. Piermarini, K. P. Choe, The multifunctional fish gill: dominant site of gas exchange, osmoregulation, acid-base regulation, and excretion of nitrogenous waste. *Physiological reviews* **85**, 97-177 (2005).
36. D. Kolosov, P. Bui, H. Chasiotis, S. P. Kelly, Claudins in teleost fishes. *Tissue barriers* **1**, e25391 (2013).
37. F. Furukawa, S. Watanabe, K. Kakumura, J. Hiroi, T. Kaneko, Gene expression and cellular localization of ROMKs in the gills and kidney of Mozambique tilapia acclimated to fresh water with high potassium concentration. *American Journal of Physiology-Regulatory, Integrative and Comparative Physiology* **307**, R1303-R1312 (2014).
38. F. Furukawa *et al.*, In vivo and in vitro effects of high-K+ stress on branchial expression of ROMKa in seawater-acclimated Mozambique tilapia. *Comparative*

Biochemistry and Physiology Part A: Molecular & Integrative Physiology **187**, 111-118 (2015).

39. W. F. Boron, Boulpaep, E.L., *Medical Physiology* (Elsevier Saunders, Philadelphia, Pennsylvania, 2005).

40. Rayleigh distillation refers to the process by which isotopes are distilled during fractionation removal (in this case uptake of K^+ through the gut endothelium). Assuming K^+ is continually removed from the system and this removal is associated with constant isotopic fractionation (a), the K isotopic composition of the residual (feces) is described by $^{41}K/^{39}K_{feces}$ /$^{41}K/^{39}K_{diet} = f^{(a-1)}$ where $^{41}K/^{39}K_{diet}$ is the ratio of K isotopes in the diet, $^{41}K/^{39}K_{feces}$ is the ratio of K isotopes in the feces, f is the fraction of K removed from the diet (80-90%), and a is the net K isotopic fractionation associated with uptake.

41. V. Garcia-Hernandez, M. Quiros, A. Nusrat, Intestinal epithelial claudins: expression and regulation in homeostasis and inflammation. *Ann. N.Y. Acad. Sci.* **1397**, 66-79 (2017).

42. M. C. Rao, "Physiology of Electrolyte Transport in the Gut: Implications for Disease" in Comprehensive Physiology. https://doi.org/10.1002/cphy.c180011, pp. 947-1023.

43. C. Terner, L. Eggleston, H. Krebs, The role of glutamic acid in the transport of potassium in brain and retina. *Biochemical Journal* **47**, 139 (1950).

44. A. W. Jones, P. D. Sander, D. L. Kampschmidt, The effect of norepinephrine on aortic ^{42}K turnover during deoxycorticosterone acetate hypertension and antihypertensive therapy in the rat. *Circulation research* **41**, 256-260 (1977).

45. D. C. Tosteson, J. F. Hoffman, Regulation of cell volume by active cation transport in high and low potassium sheep red cells. *Journal of General Physiology* **44**, 169-194 (1960).

46. J. R. Sachs, Ouabain-insensitive sodium movements in human red blood cell. *Journal of General Physiology* **57**, 259-& (1971).

47. J. Duhm, Furosemide-sensitive K+ (Rb+) transport in human-erythrocytes - modes of operation, dependence on extracellular and intracellular Na+, kinetics, pH dependency, and the effect of cell-volume and N-ethylmaleimide. *J. Membr. Biol.* **98**, 15-32 (1987).

48. G. Gardos, The function of calcium in the potassium permeability of human erythrocytes. *Biochimica et biophysica acta* **30**, 653-654 (1958).

49. S. B. Hladky, M. A. Barrand, Fluid and ion transfer across the blood–brain and blood–cerebrospinal fluid barriers; a comparative account of mechanisms and roles. *Fluids and Barriers of the CNS* **13**, 1-69 (2016).

50. R. Katzman, L. Graziani, R. Kaplan, A. Escriva, Exchange of cerebrospinal fluid potassium with blood and brain: study in normal and ouabain perfused cats. *Archives of neurology* **13**, 513-524 (1965).

51. A. L. Betz, J. A. Firth, G. W. Goldstein, Polarity of the blood-brain barrier: distribution of enzymes between the luminal and antiluminal membranes of brain capillary endothelial cells. *Brain research* **192**, 17-28 (1980).

52. S. Foroutan, J. Brillault, B. Forbush, M. E. O'Donnell, Moderate-to-severe ischemic conditions increase activity and phosphorylation of the cerebral microvascular endothelial cell Na^+-K^+-Cl^- cotransporter. *American Journal of Physiology-Cell Physiology* **289**, C1492-C1501 (2005).

53. C. Van Renterghem, P. Vigne, C. Frelin, A charybdotoxin□sensitive, Ca2+□activated K+ channel with inward rectifying properties in brain

microvascular endothelial cells: properties and activation by endothelins. *Journal of neurochemistry* **65**, 1274-1281 (1995).

54. In order to generate a negative $d^{41}K_{plasma}$ value through K isotopic fractionation associated with apical K^+ channels, 1) the rate of K^+ recycling across the basolateral membrane of collecting duct cells must be much higher than the rate of K^+ secretion and 2) the K isotope effect associated with the apical K^+ channels must be larger the K isotope effect associated with inward recycling of K^+ from collecting duct cells to plasma.

55. D. P. S. Ramos, L. A. Coogan, J. G. Murphy, J. A. Higgins, Low-temperature oceanic crust alteration and the isotopic budgets of potassium and magnesium in seawater. *Earth and Planetary Science Letters* **541**, 11 (2020).

56. E. E. Noble *et al.*, Control of Feeding Behavior by Cerebral Ventricular Volume Transmission of Melanin-Concentrating Hormone. *Cell Metab* **28**, 55-68 e57 (2018).

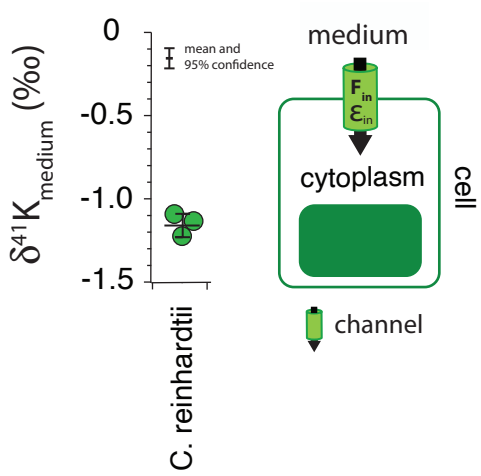

Figure 1. The difference in $\delta^{41}K$ values between external and intracellular K^+ in growth experiments of *C. reinhardtii* and a diagram of K^+ transport in single-celled algae grown under optimal conditions (See Methods) including major fluxes (F_{in}), transport machinery, and K isotope effects (ε_{in}). $P = 4.5 \times 10^{-5}$ by one-way ANOVA in Matlab.

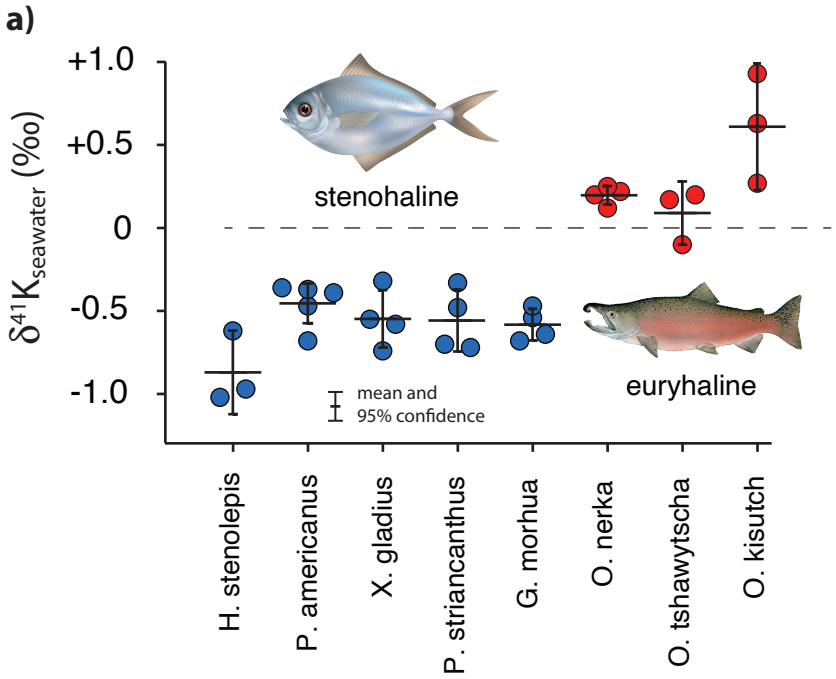

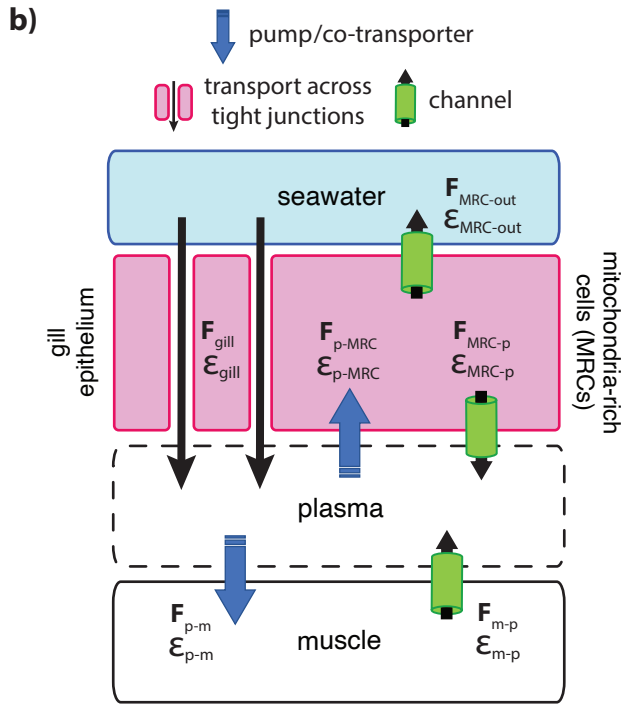

Figure 2. a) The difference in $\delta^{41}K$ values between seawater and dorsal white muscle of various stenohaline and euryhaline marine teleosts. Muscle $[K^+]$ and $\delta^{41}K_{seawater}$ values are listed in Table S1. $P = 1.4x10^{-10}$ for the difference in $\delta^{41}K_{seawater}$ value between stenohaline and euryhaline teleosts. **b)** A schematicof K isotope mass balance in a marine teleost including fluxes (F's) and isotope effects (ε's). K^+ is supplied across the gill epithelium via transport across tight-junctions and lost from mitochondrial rich cells (MRCs) through channels ($F_{MRC\text{-}out}$). K^+ cycling within MRCs reflects a balance between K^+ supplied across the basolateral membrane ($F_{p\text{-}MRC}$) and K^+ lost to seawater ($F_{MRC\text{-}out}$) and K^+ recycled back across the basolateral membrane through channels ($F_{MRC\text{-}p}$). **c)** At steady-state, $F_{gill} = F_{MRC\text{-}out}$, $F_{p\text{-}MRC} = F_{gill} + F_{MRC\text{-}p}$, $F_{p\text{-}m} = F_{m\text{-}p}$ and K isotope mass balance for teleost muscle tissue can be simplified to equation (1). One possible explanation for the elevated $\delta^{41}K_{seawater}$ values of marine euryhaline teleosts is greater recycling of K across the basolateral membrane ($f \rightarrow 1$).

c) $$\delta^{41}K^{muscle}_{seawater}\ (‰) = \varepsilon_{p\text{-}MRC} - \varepsilon_{gill} + f(\varepsilon_{MRC\text{-}out} - \varepsilon_{MRC\text{-}p}) \quad (1)$$

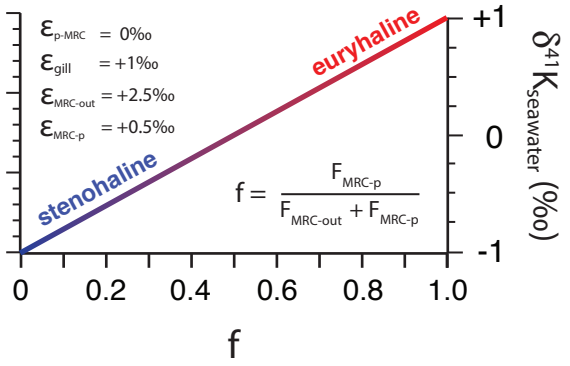

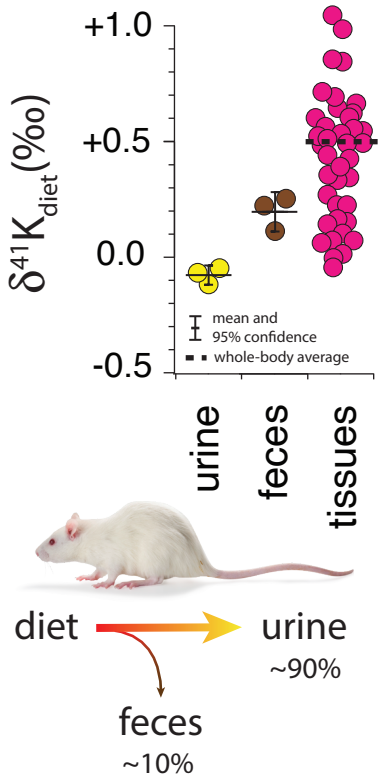

Figure 3. Whole-body K isotope mass balance in *R. norvegicus* on a controlled diet. Measured $\delta^{41}K$ values of urine ($P = 0.19$) and feces ($P = 0.037$) relative to diet indicate a preferential uptake of ^{39}K in the gut. The total range in $\delta^{41}K_{diet}$ values in the tissues of *R. norvegicus* is ~1‰ with an estimated whole-body average $\delta^{41}K_{diet}$ value of approx. +0.5‰, consistent with preferential loss of ^{39}K in urine.

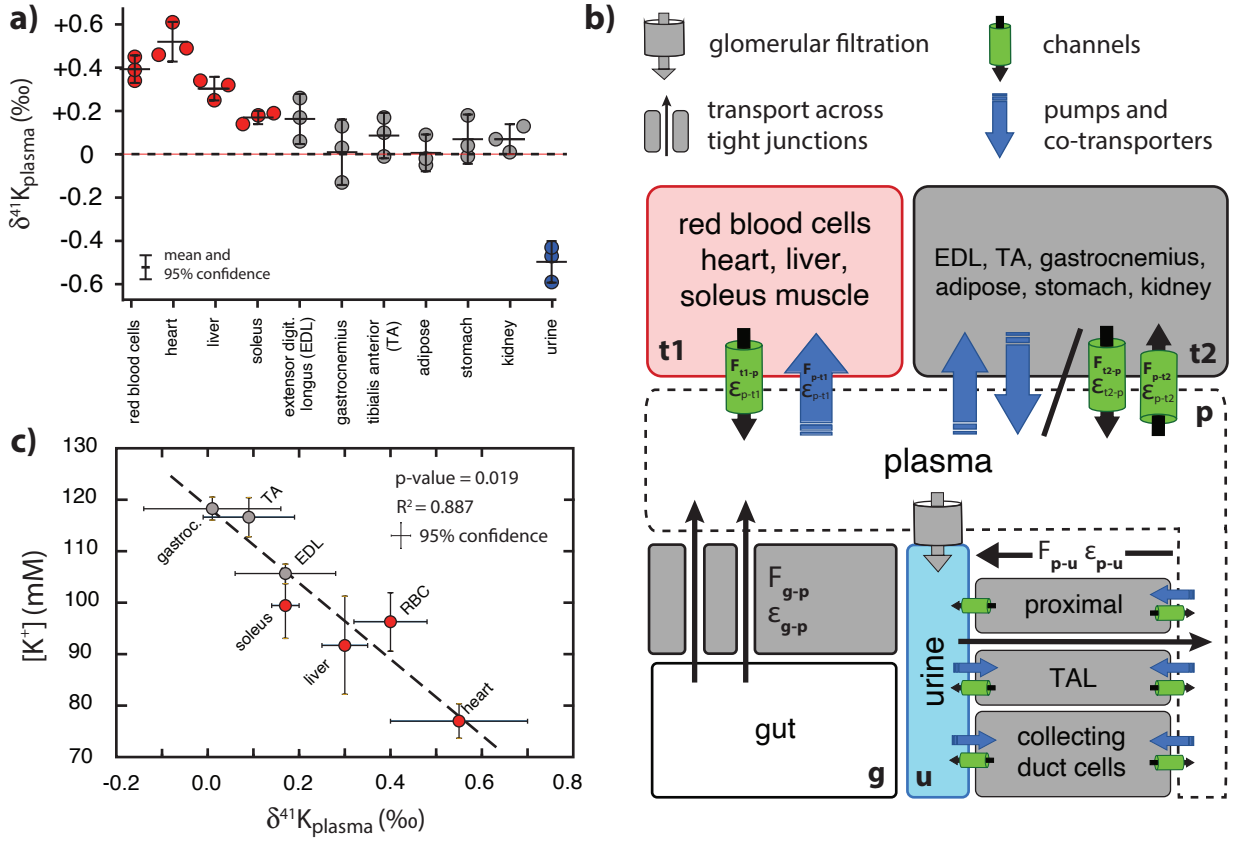

Figure 4. a) K isotopic composition of tissues/fluids *R. norvegicus* normalized to blood plasma ($\delta^{41}K_{plasma}$ = 0‰) together with **b)** a diagram of K mass-balance including transport by (1) K^+ channels, (2) K^+-pumps/co-transporters, (3) pores in tight-junctions, and (4) glomerular filtration. **c)** A plot of $[K^+]$ and $\delta^{41}K_{plasma}$ values for a subset of the tissues in *r. norvegicus* showing that tissues with lower $[K^+]$ tend to be associated with higher $\delta^{41}K_{plasma}$ values. $\delta^{41}K_{plasma}$ values that are positive (●) indicate that net K^+ transport out of the tissue/cell/fluid is enriched in ^{39}K relative to K^+ transport into the tissue/cell/fluid. $\delta^{41}K_{plasma}$ values that are indistinguishable from 0‰ (●) indicate that the K isotope effects associated with K^+ transport into and out of the cell/tissue/fluid are either 0 or equal in magnitude (and thus cancel). $\delta^{41}K_{plasma}$ values that are negative (●) indicate that net K^+ transport into the cell/tissue/fluid is enriched in ^{39}K relative to K^+ transport out of the cell/tissue/fluid. The net isotopic fractionation associated with K^+ loss in urine ($\varepsilon_{p\text{-}u}$) reflects the flux-weighted average of the K isotopic effects associated with both re-absorption and secretion of K^+ in the proximal tubule, the thick ascending limb (TAL), and cells in the collecting ducts of the kidney.

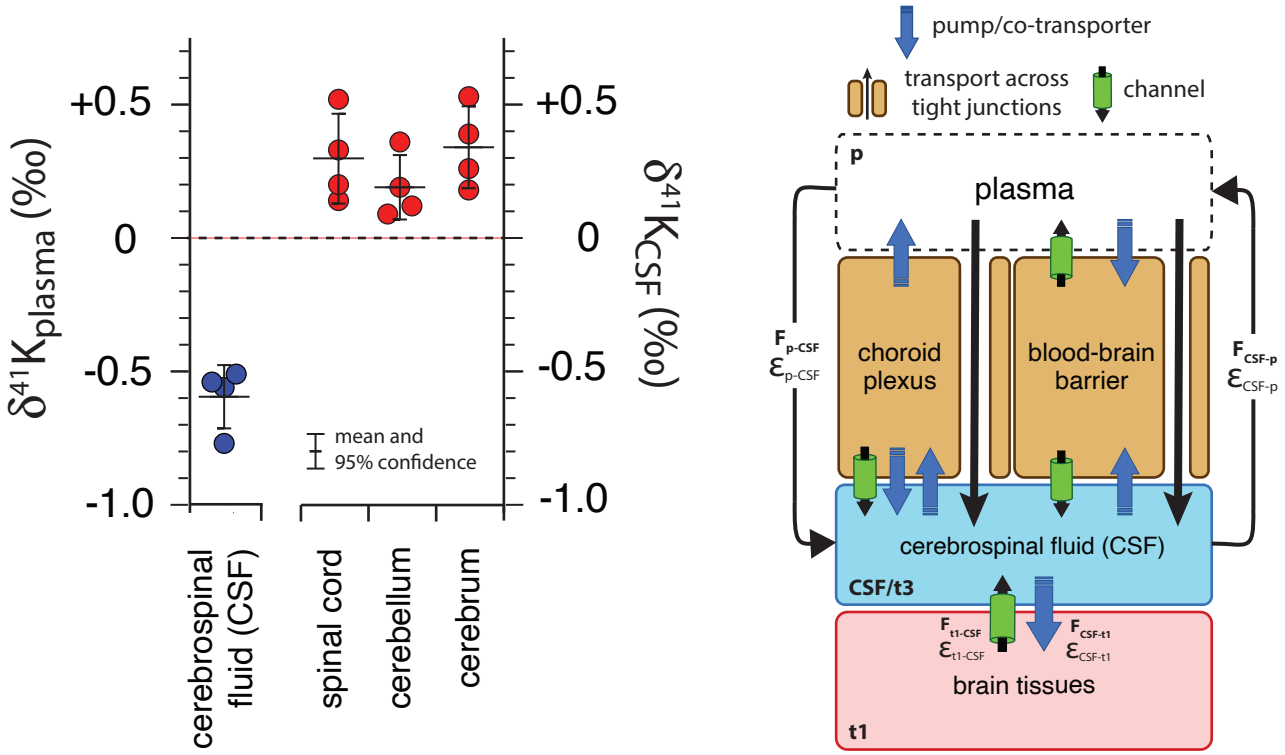

Figure 5. Potassium isotopic composition of cerebrospinalfluid from *r. norvegicus* raised on a controlled diet normalized to blood plasma ($\delta^{41}K_{plasma}$ = 0‰) and brain tissues normalized to cerebrospinal fluid ($\delta^{41}K_{CSF}$ = 0‰) together with a diagram of K mass-balance across the choroid plexus and blood brain barrier (BBB) including transport by (1) K-channels, (2) K-pumps/co-transporters, and (3) through tight junctions. K fluxes are associated with net isotope effects (ε's). $\delta^{41}K_{CSF}$ values that are positive (●) indicate that net K transport out of brain tissues (spinal cord, cerebellum, and cerebrum) and into CSF is enriched in ^{39}K relative to K transport from CSF into these tissues (e.g. $\varepsilon_{t1\text{-}CSF} - \varepsilon_{CSF\text{-}t1} > 0$) . The negative $\delta^{41}K_{plasma}$ values (●) for CSF indicate that net K transport into CSF from blood plasma is enriched in ^{39}K relative to K transport from CSF to blood plasma (e.g. $\varepsilon_{p\text{-}CSF} - \varepsilon_{CSF\text{-}p} > 0$) and reflects the flux-weighted average of the tranporters that dominate K exchange across both the chloroid plexus and BBB.